Physica D 66 (1993) 347–367
North-Holland

SDI: 0167-2789(93)E0035-I

PHYSICA D

High-order formulation of the water-wave problem

Michael Glozman, Yehuda Agnon and Michael Stiassnie

Coastal and Marine Engineering Research Institute, Faculty of Civil Engineering, Technion – Israel Institute of Technology, 32000 Haifa, Israel

Received 10 August 1992
Revised manuscript received 7 December 1992
Accepted 5 January 1993
Communicated by J.M. Ball

The water-wave problem has a Hamiltonian formulation as derived by Zakharov. This leads to coupled nonlinear evolution equations for discrete wave modes. Discrete spectra occur naturally for standing waves in a basin. For high enough order, high enough energy and a sufficient number of degrees of freedom, chaos may emerge. We have derived the Hamiltonian and evolution equations to arbitrary order. The conditions for the convergence of the expansion of the Hamiltonian are discussed. We performed numerical studies of the interaction of two standing wave modes for various cases and for increasing order. Using Poincaré sections, the onset of local chaos in resonance and near-resonance conditions is manifested. Chaos appears at low order models but vanishes with increasing order. The significance of the newly derived high-order formulation for water waves is clearly demonstrated.

1. Introduction

Ocean scientists use deterministic (implying order) as well as stochastic models to describe the nonlinear evolution of the wavy surface of the oceans, see for example the important contributions by Pierson [10], Hasselmann [6], and Yuen and Lake [14].

At least two questions stand open: (i) When should one use a deterministic or a stochastic model? (ii) Under what conditions does the actual transition from a state of order to a chaotic state (where order prevails only in the statistical sense) occur? These two questions motivated the present study, which is a step towards answering these questions.

Recently Zufiria [16] used a weakly nonlinear Hamiltonian model and showed that three traveling waves can produce chaotic behavior under certain initial conditions. Zufiria's study leaves open the important questions regarding the influence of higher order nonlinearities (finite amplitude) and a larger number of modes.

These points are of general interest. Chaotic behavior has been found in various low-order models (see [9]); the extrapolation of the results to higher order is by no means straightforward.

We will show in this paper that low-order theories can be completely misleading. They sometimes distort the real physical picture and produce apparent chaos. This chaos disappears at higher order, hence it is fictitious.

In section 2 we start from the classical water-wave problem and develop the Hamiltonian as well as the evolution equations to arbitrary order. The kernels of these equations are given by closed recursive expressions. The recursive nature of the water-wave problems requires a Hamiltonian of infinite order. This problem has been addressed by Miles [8], Benjamin [2], Dommermuth and Yue [4], West and Janda, [13] and Craig [13].

Our equations are a high-order generalization of those given by Zakharov [15] to third order and by Stiassnie and Shemer [11] to fourth order. However, in contrast to the procedure used in these two references we do not use here the multiple-time approach. This naturally leads to more time consuming computations, but enables us to circumvent intrinsic difficulties related to scale separation.

We have decided to focus on the dynamics of a standing wave system in a rectangular basin, which is naturally periodic in space, thus avoiding the additional difficulty encountered in the transition from continuous to discretized systems. In section 3 we discretize our problem for standing waves. The system of integrodifferential equations changes into a system of ordinary but highly nonlinear differential equations.

In our numerical calculation, which we present in section 4, we concentrate on the two-modes problem which enables us to use the Poincaré section technique and methodology, and study the system from a dynamical systems view point. Conclusions are given in section 5 and a convergence condition in appendix B.

Generally speaking, our results indicate that for gravity waves order five is both a reliable and economic (considering computer resources) choice.

For the two-modes case we have found that even under resonance conditions, chaos emerged locally, i.e., only in small isolated spots in the phase space. For more modes, we expect significant regions of chaos. We are currently studying the interaction of a large number of modes in higher order models.

2. Expansion to arbitrary order

2.1. Basic equations

The boundary value problem of irrotational flow of an incompressible inviscid fluid with a free surface is written in terms of a velocity potential $\varphi(x, z, t)$:

$$\Delta\varphi = 0 \quad (-h \le z \le \eta(x, t)) . \tag{2.1}$$

The origin lies on the undisturbed free surface and the z axis points vertically upwards. $x = (x, y)$ are the horizontal coordinates with two boundary conditions on the unknown free surface $\eta(x, t)$. The kinematic boundary condition:

$$\eta_t + (\nabla\varphi)\cdot(\nabla\eta) - \varphi_z = 0 \quad \text{at } z = \eta , \tag{2.2}$$

and the dynamic boundary condition:

$$\varphi_t + \tfrac{1}{2}(\nabla\varphi)^2 + \tfrac{1}{2}\varphi_z^2 + g\eta = s\,\nabla\cdot\left(\frac{\nabla\eta}{\sqrt{1+(\nabla\eta)^2}}\right) \quad \text{at } z = \eta . \tag{2.3}$$

These boundary conditions are prescribed at the unknown free surface η. As we shall see, this makes the Hamiltonian recursive.

In addition, there is a kinematic boundary condition on the horizontal bottom at depth h:

$$\varphi_z = 0 \quad \text{at } z = -h . \tag{2.4a}$$

For the case of standing waves in a basin $L_1 \times L_2$ we have

$$\varphi_x = 0 \quad \text{at } x = 0, L_1 , \tag{2.4b}$$

$$\varphi_y = 0 \quad \text{at } y = 0, L_2 . \tag{2.4c}$$

In the previous equations,

$\Delta = \partial^2/\partial x^2 + \partial^2/\partial y^2 + \partial^2/\partial z^2$ is the Laplacian, $\nabla = (\partial/\partial x, \partial/\partial y)$, is the horizontal gradient, g is the gravitational acceleration, s is the coefficient of surface tension divided by the fluid's density. We denote the potential at the free surface by $\psi(x, t) = \varphi(x, \eta(x, t), t)$.

Zakharov [15] has shown that this problem has an equivalent Hamiltonian formulation. The Hamiltonian is the total energy of the system:

$$H = T + V_g + V_c , \tag{2.5}$$

where

$$T = \tfrac{1}{2} \int_\Omega \psi \eta_t \, dx , \tag{2.6}$$

$$V_g = \tfrac{1}{2} g \int_\Omega \eta^2 \, dx , \tag{2.7}$$

$$V_c = s \int_\Omega (\sqrt{1 + (\nabla\eta)^2} - 1) \, dx . \tag{2.8}$$

Here T is the kinetic energy, V_g is the potential energy due to gravity forces, and V_c is the potential energy due to capillary forces. Ω is the horizontal region of integration. ψ and η are canonical variables and the evolution equations for the wave field are given by

$$\eta_t = \frac{\delta H}{\delta \psi} , \quad \psi_t = -\frac{\delta H}{\delta \eta} , \tag{2.9}$$

where δ stands for functional derivatives (cf. [5]). The main difficulty with this formulation is the appearance of η_t in (2.6); it will be solved in the following section. Indeed, we need to express η_t in terms of ψ and η. This can be done through a linear operator on ψ where the operator itself depends nonlinearily (to infinite order) on η. This is due to the recursive nature of the boundary value problem. Thus, the kinetic energy, T, is a quadratic function of ψ. The quantity η_t in (2.6) stands for the solution of the boundary value problem for η_t in terms of ψ and η (cf. [3]).

2.2. *Expansion of the Hamiltonian*

We assume that the solution of the Laplace equation for the finite depth case can be written through separation of variables, in the following form:

$$\varphi = \frac{1}{2\pi} \int_{-\infty}^{\infty} \hat{\Phi}(\boldsymbol{k}_0, t) \operatorname{ch}[k_0(z+h)] \, \mathrm{e}^{\mathrm{i}\boldsymbol{k}_0 \cdot \boldsymbol{x}} \, \mathrm{d}\boldsymbol{k}_0 \,, \tag{2.10}$$

$\hat{\Phi}$ is the spatial Fourier transform of $\varphi(\boldsymbol{x}, -h, t)$ and $\hat{\eta}$ is the Fourier transform of η, the free surface elevation:

$$\hat{\eta}(\boldsymbol{k}, t) = \frac{1}{2\pi} \int_{-\infty}^{\infty} \eta(\boldsymbol{x}, t) \, \mathrm{e}^{-\mathrm{i}\boldsymbol{k} \cdot \boldsymbol{x}} \, \mathrm{d}\boldsymbol{x} \,. \tag{2.11}$$

We introduce the following notations:

$$\hat{\eta}_j = \hat{\eta}(\boldsymbol{k}_j, t) \,, \quad \hat{\Phi}_0 \doteq \hat{\Phi}(\boldsymbol{k}_0, t) \,,$$

$$k = |\boldsymbol{k}| \,, \quad \mathrm{d}\boldsymbol{k}_{l \cdots m} = \prod_{i=l}^{m} \mathrm{d}\boldsymbol{k}_i \,,$$

where $\hat{\eta}(-\boldsymbol{k}, t) = \hat{\eta}^*(\boldsymbol{k}, t)$ since η is real.

From (2.10) we have for $\psi(\boldsymbol{x}, t) \equiv \varphi(\boldsymbol{x}, \eta(\boldsymbol{x}, t), t)$:

$$\psi = \frac{1}{2\pi} \int_{-\infty}^{\infty} \hat{\Phi}_0 \operatorname{ch}(k_0 \eta + k_0 h) \, \mathrm{e}^{\mathrm{i}\boldsymbol{k}_0 \cdot \boldsymbol{x}} \, \mathrm{d}\boldsymbol{k}_0 \,. \tag{2.12}$$

$$\eta^n = \prod_{j=1}^{n} \frac{1}{2\pi} \int_{-\infty}^{\infty} \hat{\eta}_j \, \mathrm{e}^{\mathrm{i}\boldsymbol{k}_j \cdot \boldsymbol{x}} \, \mathrm{d}\boldsymbol{k}_j = \frac{1}{(2\pi)^n} \int^n \exp\Big(\mathrm{i}\boldsymbol{x} \cdot \sum_{j=1}^{n} \boldsymbol{k}_j\Big) \Big(\prod_{j=1}^{n} \hat{\eta}_j\Big) \, \mathrm{d}\boldsymbol{k}_{1 \ldots n} \,, \tag{2.13}$$

where $\int^n$ stands for n integrations.

We develop $\operatorname{ch}(k_0 \eta + k_0 h)$ in a Taylor series expansion around $\eta = 0$, and express η^n by their Fourier transforms, using (2.13). We can also eliminate $\hat{\Phi}_0$ from (2.12) in terms of ψ, using recursive substitutions:

$$\hat{\Phi} \operatorname{ch}(kh) = \hat{\psi} - \sum_{q=1}^{\infty} \int^{q+1} A_q \hat{\psi}_0\Big(\prod_{m=1}^{q} \hat{\eta}_m\Big) \, \delta\Big(\boldsymbol{k} - \sum_{j=0}^{q} \boldsymbol{k}_j\Big) \, \mathrm{d}\boldsymbol{k}_{0 \ldots q} \,, \tag{2.14}$$

where the recursion expression for A_q (as well as for all other coefficients) is given in appendix A.

Similarly, we can obtain an expression for the Fourier transform of the vertical velocity at the surface $u_s = \varphi_z|_{z=\eta}$ in the form

$$\hat{u}_s = \sum_{q=0}^{\infty} \int^{q+1} B_q \hat{\psi}_0\Big(\prod_{m=1}^{q} \hat{\eta}_m\Big) \, \delta\Big(\boldsymbol{k} - \sum_{j=0}^{q} \boldsymbol{k}_j\Big) \, \mathrm{d}\boldsymbol{k}_{0 \ldots q} \,, \tag{2.15}$$

where B_q is also given in appendix A.

We rewrite (2.2), the kinematic boundary condition, in terms of ψ, the potential at the free surface:

$$\eta_t + \nabla\psi \cdot \nabla\eta - \varphi_z(1 + (\nabla\eta)^2) = 0\,, \quad z = \eta\,. \tag{2.16}$$

Taking the Fourier transform of (2.16) and utilizing (2.15), after some manipulation leads to

$$\hat{\eta}_t = \sum_{q=0}^{\infty} \int^{q+1} C_q \hat{\psi}_0 \Big(\prod_{m=1}^{q} \hat{\eta}_m \Big)\, \delta\Big(\boldsymbol{k} - \sum_{j=0}^{q} \boldsymbol{k}_j \Big)\, \mathrm{d}\boldsymbol{k}_{0\ldots q}\,. \tag{2.17}$$

The kinetic energy is then readily calculated from (2.6)

$$\begin{aligned} T &= \tfrac{1}{2} \int \psi\eta_t \,\mathrm{d}\boldsymbol{x} = \frac{1}{2}\,\frac{1}{(2\pi)^2} \int_{-\infty}^{\infty} \int\int \hat{\psi}_0 \hat{\eta}_t\, \mathrm{e}^{\mathrm{i}\boldsymbol{x}\cdot(\boldsymbol{k}_0+\boldsymbol{k})}\, \mathrm{d}\boldsymbol{k}\, \mathrm{d}\boldsymbol{k}_0\, \mathrm{d}\boldsymbol{x} \\ &= \tfrac{1}{2} \int_{-\infty}^{\infty} \int \hat{\psi}_0 \hat{\eta}_t\, \delta(\boldsymbol{k}_0 + \boldsymbol{k})\, \mathrm{d}\boldsymbol{k}_0\, \mathrm{d}\boldsymbol{k} = \tfrac{1}{2} \int_{-\infty}^{\infty} \hat{\psi}(-\boldsymbol{k})\, \hat{\eta}_t(\boldsymbol{k})\, \mathrm{d}\boldsymbol{k}\,. \end{aligned} \tag{2.18}$$

Similarly,

$$V_g = \tfrac{1}{2} g \int \eta^2 \,\mathrm{d}\boldsymbol{x} = \tfrac{1}{2} g \int_{-\infty}^{\infty} \hat{\eta}(\boldsymbol{k})\, \hat{\eta}(-\boldsymbol{k})\, \mathrm{d}\boldsymbol{k}\,. \tag{2.19}$$

For V_c (2.8) we perform a Taylor series expansion and take Fourier transforms, which yield:

$$V_c = -s \sum_{n=1}^{\infty} \frac{\beta_n'}{(2\pi)^{2n-2}} \int^{2n} \prod_{m=1}^{n} (\boldsymbol{k}_{2m-1} \cdot \boldsymbol{k}_{2m}) \Big(\prod_{m=1}^{2n} \hat{\eta}_m \Big) \delta\Big(\sum_{j=1}^{2n} \boldsymbol{k}_j \Big)\, \mathrm{d}\boldsymbol{k}_{1\ldots 2n}\,. \tag{2.20}$$

Following Zakharov, we apply the following linear transformation changing from η, ψ to the new variables $a(k)$ and $a^*(-k)$:

$$\hat{\eta}(\boldsymbol{k}) = \frac{1}{\sqrt{2}}\, \lambda(\boldsymbol{k})\, [a(\boldsymbol{k}) + a^*(-\boldsymbol{k})]\,, \qquad \mathrm{i}\hat{\psi}(\boldsymbol{k}) = \frac{1}{\sqrt{2}}\, \xi(\boldsymbol{k})\, [a(\boldsymbol{k}) - a^*(-\boldsymbol{k})]\,, \tag{2.21}$$

so that

$$a(\boldsymbol{k}) = \frac{\hat{\eta}(\boldsymbol{k})}{\sqrt{2}\,\lambda(\boldsymbol{k})} + \mathrm{i}\,\frac{\hat{\psi}(\boldsymbol{k})}{\sqrt{2}\,\xi(\boldsymbol{k})}\,, \tag{2.22a}$$

where

$$\lambda = \lambda(k) = \left(\frac{k\,\mathrm{th}(kh)}{\omega(k)} \right)^{1/2} = \frac{1}{\xi}\,. \tag{2.22b}$$

The frequency $\omega(k)$ is given by the linear theory dispersion relation

$$\omega^2 = (gk + sk^3)\,\mathrm{th}(kh)\,. \tag{2.22c}$$

After some further algebra we can write the components of the Hamiltonian (2.5) in terms of $a(\boldsymbol{k})$ as follows:

$$T = -\tfrac{1}{4}\int_{-\infty}^{\infty} \frac{1}{\lambda}\,[a(-k) - a^*(k)] \sum_{q=0}^{\infty} \int^{q+1} C_q \frac{1}{\lambda_0}\,(a_0 - a^*_{-0})\,\frac{1}{2^{q/2}}$$

$$\times \Big(\prod_{m=1}^{q} \lambda_m (a_m + a^*_{-m})\Big)\,\delta\Big(k - \sum_{j=0}^{q} k_j\Big)\,\mathrm{d}k\,\mathrm{d}k_{0\ldots q}\,,$$

$$V_g = \tfrac{1}{4} g \int_{-\infty}^{\infty} \lambda^2 [a(k) + a^*(-k)][a(-k) + a^*(k)]\,\mathrm{d}k\,,$$

$$V_c = \tfrac{1}{4} s \int_{-\infty}^{\infty} \lambda\,[a(-k) + a^*(k)] \sum_{q=0}^{\infty} \int^{q+1} \frac{G_{q/2}}{2^{q/2}(\frac{1}{2}q+1)} \Big(\prod_{m=0}^{q} \lambda_m (a_m + a^*_{-m})\Big)\,\delta\Big(k - \sum_{j=0}^{q} k_j\Big)\,\mathrm{d}k\,\mathrm{d}k_{0\ldots q}\,,$$

where $a_m = a(k_m)$. (2.23)

This way,

$$H = H(a(k), a^*(k), a(-k), a^*(-k))\,.$$

The Hamiltonian which has been derived here to arbitrary order in (2.23) is substituted in eq. (2.9) which leads to the following evolution equation:

$$a_t(k) = -\mathrm{i}\,\frac{\delta H}{\delta a^*(k)}\,. \tag{2.24}$$

2.3. *Independent derivation of the evolution equations*

We may also derive the evolution equations (2.24) in an alternative way, following Yuen and Lake [14].

The equation for η_t is given as before by (2.17). Writing the dynamic boundary condition (2.3), in terms of ψ we obtain

$$\psi_t + \tfrac{1}{2}(\nabla\psi)^2 - \tfrac{1}{2}\varphi_z^2(1 + (\nabla\eta)^2 + g\eta = F_c\,, \tag{2.25}$$

where F_c is the capillary term on the rhs of (2.3).

Using the same techniques as before and performing the necessary transformations, we obtain the evolution equations in the form

$$\hat{\eta}_t = k\hat{\psi}\,\mathrm{th}(kh) + \sum_{q=1}^{\infty} \int^{q+1} C_q \hat{\psi}_0 \Big(\prod_{m=1}^{q} \hat{\eta}_m\Big)\,\delta\Big(k - \sum_{j=0}^{q} k_j\Big)\,\mathrm{d}k_{0\ldots q}\,,$$

$$\hat{\psi}_t = -g\hat{\eta} - sk^2\hat{\eta} + \tfrac{1}{2}\sum_{q=0}^{\infty} \int^{q+2} D_q \hat{\psi}_0 \hat{\psi}_{q+1} \Big(\prod_{m=1}^{q} \hat{\eta}_m\Big)\,\delta\Big(k - \sum_{j=0}^{q+1} k_j\Big)\,\mathrm{d}k_{0\ldots(q+1)}$$

$$- s \sum_{q'=1}^{\infty} \int^{2q'+1} G_{q'} \Big(\prod_{m=0}^{2q'} \hat{\eta}_m\Big)\,\delta\Big(k - \sum_{j=0}^{2q'} k_j\Big)\,\mathrm{d}k_{0\ldots 2q'}\,, \tag{2.26}$$

where the coefficients C_q, D_q and G_q are given in appendix A.

Using (2.21) we can rewrite (2.26) as one equation for $a(\boldsymbol{k})$:

$$a_t(\boldsymbol{k}) + \mathrm{i}\omega(k)\, a(\boldsymbol{k}) = -\frac{\mathrm{i}}{2\lambda} \sum_{q=1}^{\infty} \int^{q+1} C_q \frac{1}{\lambda_0} (a_0 - a^*_{-0}) \frac{1}{2^{q/2}} \Big(\prod_{m=1}^{q} \lambda_m\Big)\Big(\prod_{m=1}^{q} (a_m + a^*_{-m})\Big)$$
$$\times \delta\Big(\boldsymbol{k} - \sum_{j=0}^{q} \boldsymbol{k}_j\Big)\, \mathrm{d}\boldsymbol{k}_{0\ldots q}$$
$$- \frac{\mathrm{i}\lambda}{4\sqrt{2}} \sum_{q=0}^{\infty} \int^{q+2} D_q \frac{(a_0 - a^*_{-0})(a_{(q+1)} - a^*_{-(q+1)})}{2^{q/2}\lambda_0\lambda_{(q+1)}} \Big(\prod_{m=1}^{q} \lambda_m\Big)\Big(\prod_{m=1}^{q} (a_m + a^*_{-m})\Big)$$
$$\times \delta\Big(\boldsymbol{k} - \sum_{j=0}^{q+1} \boldsymbol{k}_j\Big)\, \mathrm{d}\boldsymbol{k}_{0\ldots(q+1)}$$
$$- \tfrac{1}{2}\mathrm{i}s\lambda \sum_{q=1}^{\infty} \int^{2q+1} G_q \frac{1}{2^q} \Big(\prod_{m=0}^{2q} \lambda_m\Big)\Big(\prod_{m=0}^{2q} (a_m + a^*_{-m})\Big)\, \delta\Big(\boldsymbol{k} - \sum_{j=0}^{2q} \boldsymbol{k}_j\Big)\, \mathrm{d}\boldsymbol{k}_{0\ldots 2q}\,. \tag{2.27}$$

We will check, in section 3, the agreement between the evolution equation (2.27) and the one obtained from the Hamiltonian (2.23), (2.24). In the sequel we shall focus our attention on standing waves. Thus we continue by discretizing the evolution equations.

3. Discretization for standing waves

3.1. General form

For standing waves, in a finite basin of dimensions L_1 and L_2, (2.4b), (2.4c) apply, hence the wavenumber spectrum is discrete. Thus, instead of Fourier transforms, we use Fourier series. We may obtain the components of the Hamiltonian in a simple form, closest to the form we used in the Fourier transform notation, by using the following formulas for the Fourier decomposition.

For the two-dimensional case the Fourier series is written in terms of

$$\hat{f}(\boldsymbol{k}_{lm}) = \frac{1}{4\sqrt{L_1 L_2}} \int_{-L_1-L_2}^{L_1 L_2} f(\boldsymbol{x})\, \mathrm{e}^{-\mathrm{i}\boldsymbol{k}_{lm}\cdot\boldsymbol{x}}\, \mathrm{d}x_1\, \mathrm{d}x_2 \tag{3.1}$$

as follows:

$$f(\boldsymbol{x}) = \frac{1}{\sqrt{L_1 L_2}} \sum_{\substack{l,m=-\infty \\ (l,m)\neq(0,0)}}^{\infty} \hat{f}(\boldsymbol{k}_{lm})\, \mathrm{e}^{\mathrm{i}\boldsymbol{k}_{lm}\cdot\boldsymbol{x}}\,, \tag{3.2}$$

where $\boldsymbol{x} = (x, y)$; $\boldsymbol{k}_{lm} = (k_l, k_m)$ is discrete, with

$$k_l = \frac{\pi l}{L_1}\,, \quad k_m = \frac{\pi m}{L_2}\,, \quad l, m = 0, \pm 1, \pm 2 \ldots. \tag{3.3}$$

Note that $(l, m) \neq (0, 0)$ because there is no mean motion.

In the case of standing waves we also have due to the boundary conditions (2.4b), (2.4c) the following symmetry requirements:

$$a(k_l, k_m) = a(-k_l, k_m) = a(k_l, -k_m) = a(-k_l, -k_m)\,, \tag{3.4}$$

and (3.1) can be written as a cosine series.

For the one-dimensional case we write the Fourier expansion as follows:

$$\hat{f}(k_l) = \frac{1}{2\sqrt{L1}} \int_{-L_1}^{L_1} f(x)\, \mathrm{e}^{-\mathrm{i}k_l x}\, \mathrm{d}x\,, \tag{3.5}$$

$$f(x) = \frac{1}{\sqrt{L_1}} \sum_{\substack{l=-\infty \\ \neq}}^{\infty} \hat{f}(k_l)\, \mathrm{e}^{\mathrm{i}k_l x}\,. \tag{3.5a}$$

The application of the forms we use for the Fourier transforms and Fourier series ensures that in all the cases the structure of the equations remains the same, and only some numerical multiplier in the coefficients A, B, C, D, G must be changed.

In order to obtain compact expressions, we introduce additional notations:

$$\boldsymbol{k}_{l_j p_j} = (k_{l_j}, k_{p_j})\,, \tag{3.6}$$

where

$$k_{l_j} = \frac{\pi l_j}{L_1}\,, \quad l_j = 0, \pm 1, \pm 2\,, \qquad k_{p_j} = \frac{\pi p_j}{L_2}\,, \quad p_j = 0, \pm 1, \pm 2\,. \tag{3.7}$$

We also use the following short notations:

$$\boldsymbol{k}_j = (k_{l_j}, k_{p_j})\,, \quad \boldsymbol{k} = (k_l, k_p)\,, \quad a = a(\boldsymbol{k})\,, \quad a_m = a(\boldsymbol{k}_m)\,,$$

$$\hat{\eta}_m = \hat{\eta}(\boldsymbol{k}_m)\,, \quad \hat{\psi}_m = \hat{\psi}(\boldsymbol{k}_m)\,, \quad \lambda_m = \lambda(\sqrt{k_{l_m}^2 + k_{p_m}^2})\,, \qquad \lambda = \lambda(k) = \lambda(\sqrt{k_l^2 + k_p^2})\,, \tag{3.8}$$

$$2R_m = a_m + a_m^*\,, \quad 2\mathrm{i}I_m = a_m - a_m^*\,, \qquad 2R = a + a^*\,, \quad 2\mathrm{i}I = a - a^*\,, \tag{3.9}$$

$$\overbrace{\sum_{l_0=-\infty}^{\infty} \cdots \sum_{l_q=-\infty}^{\infty}}^{q+1} \to \overbrace{\sum_{l_0 \ldots q=-\infty}^{\infty}}^{q+1}\,. \tag{3.10}$$

Using these notations we can write the evolution equation (2.27) for standing waves in the following form:

$$\begin{aligned} a_t(\boldsymbol{k}) + \mathrm{i}\omega(k)\, a(\boldsymbol{k}) = {} & \frac{1}{\lambda} \sum_{q=1}^{\infty} 2^{q/2} \overbrace{\sum_{l_0 \ldots q=-\infty}^{\infty}}^{q+1} \overbrace{\sum_{p_0 \ldots q=-\infty}^{\infty}}^{q+1} C_q \frac{1}{\lambda_0} I_0 \Big(\prod_{m=1}^{q} \lambda_m \Big) \Big(\prod_{m=1}^{q} R_m \Big)\, \delta\Big[\boldsymbol{k}, \sum_{j=0}^{q} \boldsymbol{k}_j\Big] \\ & + \frac{\mathrm{i}\lambda}{\sqrt{2}} \sum_{q=0}^{\infty} 2^{q/2} \overbrace{\sum_{l_0 \ldots q+1=-\infty}^{\infty}}^{q+2} \overbrace{\sum_{p_0 \ldots q+1=-\infty}^{\infty}}^{q+2} D_q \frac{I_0 I_{q+1}}{\lambda_0 \lambda_{q+1}} \Big(\prod_{m=1}^{q} \lambda_m \Big) \Big(\prod_{m=1}^{q} R_m \Big)\, \delta\Big[\boldsymbol{k}, \sum_{j=0}^{q+1} \boldsymbol{k}_j\Big] \\ & - \mathrm{i}s\lambda \sum_{q=1}^{\infty} 2^q \overbrace{\sum_{l_0 \ldots 2q=-\infty}^{\infty}}^{2q+1} \overbrace{\sum_{p_0 \ldots 2q=-\infty}^{\infty}}^{2q+1} G_q \Big(\prod_{m=0}^{2q} \lambda_m \Big) \Big(\prod_{m=0}^{2q} R_m \Big)\, \delta\Big[\boldsymbol{k}, \sum_{j=0}^{2q} \boldsymbol{k}_j\Big]\,. \end{aligned} \tag{3.11}$$

Note that $\boldsymbol{k}_j \neq \boldsymbol{0}$ everywhere and that δ is Kronecker's delta

$$\delta[\boldsymbol{k}, \boldsymbol{k}'] = \begin{cases} 0 & \boldsymbol{k} \neq \boldsymbol{k}' , \\ 1 & \boldsymbol{k} = \boldsymbol{k}' . \end{cases}$$

For the restricted one-dimensional case, after some transformation we have

$$\begin{aligned} a_t(k_l) + \mathrm{i}\omega(k_l)a(k_l) = {} & \frac{1}{\lambda} \sum_{q=1}^{N} \sum_{\substack{l_0 \ldots q = -M \\ \neq 0}}^{\overbrace{M}^{q+1}} C_q \frac{1}{\lambda_0} I_0 2^{q/2} \Big(\prod_{m=1}^{q} \lambda_m \Big) \Big(\prod_{m=1}^{q} R_m \Big) \delta\Big[k_l, \sum_{j=0}^{q} k_{l_j} \Big] \\ & + \tfrac{1}{2}\mathrm{i}\lambda \sum_{q=1}^{N} \sum_{\substack{l_0 \ldots q = -M \\ \neq 0}}^{\overbrace{M}^{q+1}} D_{q-1} \frac{I_0 I_q}{\lambda_0 \lambda_q} 2^{q/2} \Big(\prod_{m=1}^{q-1} \lambda_m \Big) \Big(\prod_{m=1}^{q-1} R_m \Big) \delta\Big[k_l, \sum_{j=0}^{q} k_{l_j} \Big] \\ & - \mathrm{i}s\lambda \sum_{q=1}^{N} \sum_{\substack{l_0 \ldots q = -M \\ \neq 0}}^{\overbrace{M}^{q+1}} G_{q/2} 2^{q/2} \Big(\prod_{m=0}^{q} \lambda_m \Big) \Big(\prod_{m=0}^{q} R_m \Big) \delta\Big[k_l, \sum_{j=0}^{q} k_{lj} \Big] . \end{aligned} \tag{3.12}$$

The corresponding equations for the components of the Hamiltonian (2.23) are

$$\begin{aligned} T = {} & -\tfrac{1}{4} \sum_{\substack{l=-M \\ \neq 0}}^{M} \frac{1}{\lambda} [a(-k_l) - a^*(k_l)] \sum_{q=0}^{N} \sum_{\substack{l_0 \ldots q = -M \\ \neq 0}}^{\overbrace{M}^{q+1}} \frac{C_q}{2^{q/2}\lambda_0} (a_0 - a^*_{-0}) \\ & \times \Big(\prod_{m=1}^{q} \lambda_m \Big) \Big(\prod_{m=1}^{q} (a_m + a^*_{-m}) \Big) \delta\Big[k_l, \sum_{j=0}^{q} k_{l_j} \Big] , \\ V_{\mathrm{g}} = {} & \tfrac{1}{4} g \sum_{\substack{l=-M \\ \neq 0}}^{M} \lambda^2 [a(k_l) + a^*(-k_l)][a(-k_l) + a^*(k_l)] , \\ V_{\mathrm{c}} = {} & \tfrac{1}{4} s \sum_{\substack{l=-M \\ \neq 0}}^{M} \lambda [a(-k_l) + a^*(k_l)] \sum_{q=0}^{N} \sum_{\substack{l_0 \ldots q = -M \\ \neq 0}}^{\overbrace{M}^{q+1}} \frac{G_{q/2}}{2^{q/2}(\frac{1}{2}q + 1)} \Big(\prod_{m=0}^{q} \lambda_m \Big) \\ & \times \Big(\prod_{m=0}^{q} (a_m + a^*_{-m}) \Big) \delta\Big[k_l, \sum_{j=0}^{q} k_{l_j} \Big] . \end{aligned} \tag{3.13}$$

The Hamiltonian equation (2.24) becomes

$$a_t(k) = -\mathrm{i} \frac{\partial H}{\partial a^*(k)} . \tag{3.14}$$

In terms of R and I, defined in (3.9), eqs. (3.14) and (3.13) yield

$$R_t(k_m) = \frac{1}{4} \frac{\partial H}{\partial I(k_m)} , \quad I_t(k_m) = -\frac{1}{4} \frac{\partial H}{\partial R(k_m)} , \tag{3.15}$$

$$T = 2\sum_{l=1}^{M}\frac{1}{\lambda}I_l\sum_{q=0}^{N}\sum_{l_0\ldots\overset{q+1}{\overbrace{M}}\neq 0}^{q=-M} C_q\frac{1}{\lambda_0}I_0 2^{q/2}\Big(\prod_{m=1}^{q}\lambda_m\Big)\Big(\prod_{m=1}^{q}R_m\Big)\delta\Big[k_l,\sum_{j=0}^{q}k_{l_j}\Big], \tag{3.16}$$

$$V_g = 2g\sum_{l=1}^{M}\lambda^2 R_l^2,$$

$$V_c = 2s\sum_{l=1}^{M}\lambda R_l\sum_{q=0}^{N}\sum_{l_0\ldots\overset{q+1}{\overbrace{M}}\neq 0}^{q=-M}\frac{G_{q/2}}{\frac{1}{2}q+1}2^{q/2}\Big(\prod_{m=0}^{q}\lambda_m\Big)\Big(\prod_{m=0}^{q}R_m\Big)\delta\Big[k_l,\sum_{j=0}^{q}k_{l_j}\Big]. \tag{3.17}$$

3.2. Truncation to a two-modes model

Any computation has to be performed for a finite number of modes. The simplest interesting case is that of two modes. This is a system of two degrees of freedom with one real conserved quantity, the Hamiltonian. We expect chaos to emerge in this system. In this section we write the equations for a system of two modes. We found that the two independent derivations of the evolution equations given in sections 2.2 and 2.3 yield the same result.

Denoting $I_i = I(k_i) = I(-k_i)$, $R_i = R(k_i) = R(-k_i)$, $i = 1, 2$; computing in (3.12), (3.16) and (3.17) the coefficients and collecting terms of similar structure, we have

$$a_t(k_i) + \mathrm{i}\omega(k_i)\,a(k_i) = \sum_{j=2}^{N}\Bigg(\sum_{l=0}^{1}\sum_{m=0}^{j-1}C_{ijlm}I_2^l I_1^{1-l}R_2^m R_1^{j-1-m} + \mathrm{i}\sum_{l=0}^{2}\sum_{m=0}^{j-2}D_{ijlm}I_2^l I_1^{2-l}R_2^m R_1^{j-2-m} + \mathrm{i}\sum_{m=0}^{j}G_{ijm}R_2^m R_1^{j-m}\Bigg), \tag{3.18}$$

$$T = \sum_{j=1}^{N}\sum_{l=0}^{2}\sum_{m=0}^{j-1}E_{jlm}I_2^l I_1^{2-l}R_2^m R_1^{j-1-m}, \tag{3.19}$$

$$V = V_g + V_c = \sum_{j=1}^{N}\sum_{m=0}^{j+1}V_{jm}R_2^m R_1^{j+1-m}, \tag{3.20}$$

where $i = 1, 2$ is the equation number, $j = 1, 2, \ldots$ is the order of the term, $l = 0, 1(2)$ is the power of I_2, $m = 0, 1, \ldots$ is the power of R_2.

The coefficients E and V in the expressions for the kinetic and potential energy respectively are given in terms of C and G, as follows:

$$\begin{aligned}
&j = 1{:}\ E_{100} = 2\omega_1,\quad E_{110} = 0,\quad E_{120} = 2\omega_2,\\
&j > 1{:}\ E_{j0m} = 2C_{1j0m},\quad E_{j1m} = 2(C_{1jlm} + C_{2j0m}),\quad E_{j2m} = 2C_{2j1m},
\end{aligned} \tag{3.21}$$

$$\begin{aligned}
&j = 1{:}\ V_{10} = 2\omega_1,\quad V_{11} = 0,\quad V_{12} = 2\omega_2,\\
&j > 1{:}\ V_{j0} = -\frac{4}{j+1}G_{1j0},\quad V_{j(j+1)} = -\frac{4}{j+1}G_{2jj},\\
&m = 1\ldots j{:}\ V_{jm} = -\frac{4}{j+1}(G_{1jm} + G_{2j(m-1)}).
\end{aligned} \tag{3.22}$$

Taking derivatives of $H = T + V$ according to (3.15) and comparing with (3.18) we recover the same connections as above (3.21), (3.22) which verifies the independently derived evolution equation. In addition this procedure leads to the following symmetry properties of the coefficients:

$$C_{1j1m} = C_{2j0m}, \quad D_{1jlm} = \tfrac{1}{2}(j-1-m)(C_{1jlm} + C_{2j(l-1)m}), \quad D_{2jl(m-1)} = -\tfrac{1}{2}m(C_{1jlm} + C_{2j(l-1)m}),$$
$$\frac{D_{1jlm}}{D_{2jl(m-1)}} = \frac{j-1-m}{m}, \quad \frac{G_{1jm}}{G_{2j(m-1)}} = \frac{j+1-m}{m}. \tag{3.23}$$

Numerical computations of the coefficients C, D, G, which were performed using the general formulas, given in appendix A, show, that all the relations between the above mentioned coefficients, (3.21), (3.22), (3.23) hold exactly. In appendix B we discuss the question of convergence of the series for the Hamiltonian and derive a necessary condition. In the next chapter we turn to some examples that justify the need for higher order expansions.

4. Some examples

4.1. Numerical and graphical methods

The high-order expressions for the evolution of standing waves are very well suited for numerical simulations. For this purpose, a special software package was designed. All the programs are written in FORTRAN-77 in double precision. The first program computes the relevant interaction coefficients up to any prescribed order and collects the terms, so that the output gives the coefficients C, D and G in (3.18) as well as E and V in (3.19) and (3.20). The input parameters for this program are: basin dimensions, modes' numbers and prescribed order.

The second program ("scanner") solves the systems (3.18), using the coefficients from the first program (up to the prescribed order). The scanner constructs Poincaré sections $I_2 = 0$ or $I_1 = 0$ on the surface of a Hamiltonian with a prescribed magnitude. The system (3.18), which is a system of four real differential equations, is integrated, using the standard Runge-Kutta sixth-order solver, with relative error about 10^{-10}. This solver permits high-precision integration in both directions, and we explicitly use Brent's algorithm in order to obtain the points at which the trajectory intersects the surface, say $I_2 = 0$. Our approach is slightly different from the conventional: we compute all points of intersection, upwards as well as downwards, but we put them in two different files.

Our original phase space is four-dimensional. A section such as $I_2 = 0$ gives a three-dimensional subspace. The Hamiltonian, which is constant in time, defines a closed surface in this subspace, and all intersection points to this surface ("Hamiltonian surface"). One part of the Hamiltonian surface, for which $\partial H/\partial R_2 > 0$, corresponds to interaction points $(I_2)_t < 0$ ("intersection downwards"), the other part, for which $\partial H/\partial R_2 < 0$, corresponds to intersection points with $(I_2)_t > 0$ ("intersection upwards"). On the boundary between the above two parts, i.e., on the equator of the Hamiltonian surface intersection is impossible. Our two files of intersection points relate to the two parts of the Hamiltonian surface.

This permits us to project separately each part of the Hamiltonian surface (actually the intersection points, which lie on this part) on the plane I_1–R_1 (I_2–R_2) giving the $I_2 = 0$ ($I_1 = 0$) section.

In fig. 1 we see two sections $I_1 = 0$, $I_2 = 0$ at orders 4 and 5. The discussion about the effect of the order will be given later.

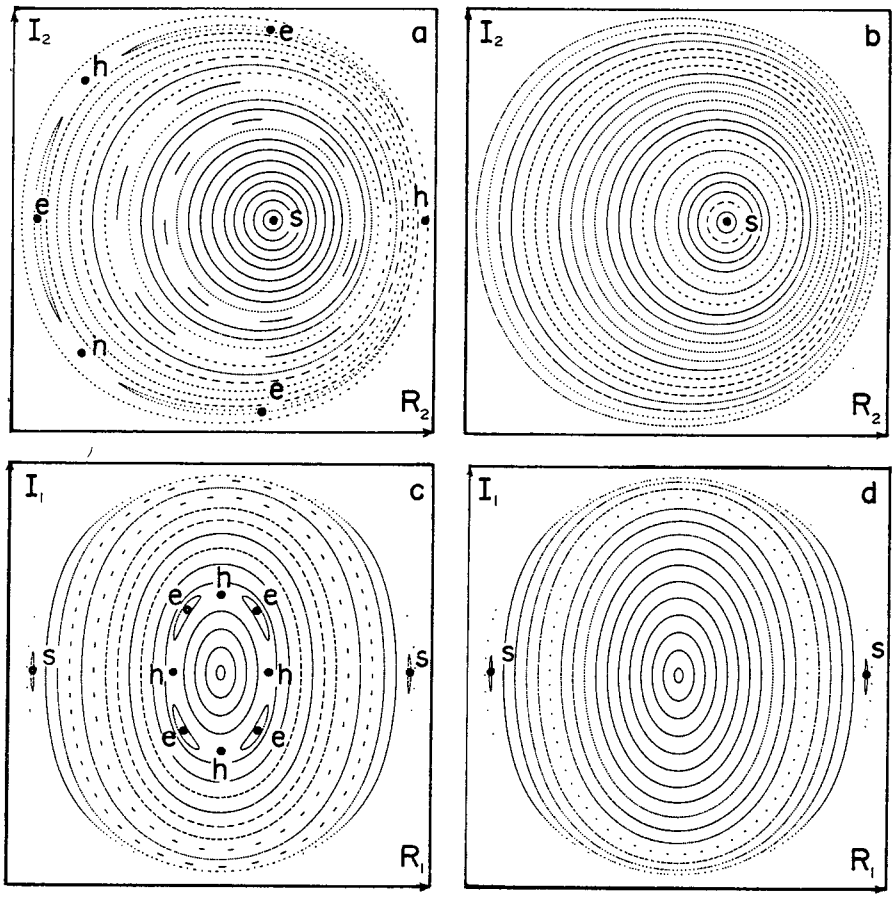

Fig. 1. Poincaré sections at different orders. $H = 0.97H_c$, $k_2 = 2k_1$, $\omega_2 = \sqrt{2}\,\omega_1$. (a), (b) $I_1 = 0$ section at order 4, 5. (c), (d) $I_2 = 0$ section at order 4, 5. Notation of selected points: e – elliptic, h – hyperbolic, s – elliptic point associated with the Stokes wave.

The purpose of the scanner is to create a set of trajectories which covers the whole Hamiltonian surface, and thereby gives the full picture of the motion for various initial conditions. Several modes of scanning are available; usually 17 initial points are located on an arc of prescribed radius or on a prescribed straight line. The result is two files; each of them contains 10 200 points of intersection – 600 points for each trajectory. In order to check the global error, we also compute the value of the Hamiltonian for each point of intersection. For the initial points only two coordinates are given, the third coordinate is computed, using the prescribed value of the Hamiltonian. Thus, the cumulative error at the end of each trajectory is an algebraic sum of the error in the computed coordinate of the initial point, and the global error of integration. For the wide range of computations, which were performed using various wavelengths, Hamiltonian values, initial points and lengths of trajectory (up to 5 000 points of intersection) the terminal value of the Hamiltonian had at least 8 accurate significant digits. This means that we can be sure, that in our output, all of the retained 6 significant digits, are accurate. With such a number of significant digits, our output is equivalent to a matrix picture with $10^6 \times 10^6$ pixels.

Note that for the initial point ($I_1 = 0$, $R_1 = 0$) we have a trajectory, which gives only one point of intersection – the same point ($I_1 = 0$, $R_1 = 0$). This means that if in our two-mode system at $t = 0$ all the energy is concentrated in the second mode, nonlinear interactions between the modes are impossible. Such points appear in every system with a limited number of modes.

4.2. Convergence and fictitious chaos at low orders

Our problem is described by a system of ordinary differential equations, where the rhs are infinite series. All practical models use truncated series, and thus the question of convergence of these rhs is very important.

In appendix B we have derived an analytic convergence criterion for an individual mode. Deriving such a criterion for the whole system seems to be very difficult. Another approach is possible. Using our package, we directly study the convergence of solutions of different orders. Of course, we do not know the exact solution, but we can check the convergence in the Cauchy sense. We compared scans of different orders, obtained for the same Hamiltonian and the same set of initial points. When the differences between successive scans diminished with increasing order, we concluded that the series converges.

For instance, the convergence of the location (R_1, R_2) of the period 2 periodic point, denoted by the letter s in fig. 1, is clearly demonstrated in table 1.

The orders given in this table and elsewhere refer to the rhs of the evolution equations (3.18). Note that the appropriate Hamiltonian is one order higher.

In the rightmost column of table 1 we give the value of the residue at the point s. The value of the residue is an indication of the linear stability of a periodic point of the map. For an elliptic point the residue is in the range (0, 1), see [7].

According to our criterion for individual modes (see appendix B), the relative amplitude, i.e., the amplitude to wavelength ratio of each mode cannot exceed the critical value $\varepsilon_c = 1/2\pi$. Denoting the relative amplitudes of the modes by ε_1, ε_2, we define $\varepsilon_{max} = \max(\varepsilon_1, \varepsilon_2)$, where the maximum is taken over the whole Hamiltonian surface. We denote the value of the Hamiltonian, for which $\varepsilon_{max} = \varepsilon_c$ by H_c.

Our conclusion from various computations for gravity waves is that the fifth order is the optimal order of solution leading to results with average error (1–2)% in the location of the periodic orbit (Stokes wave).

By examining fig. 1 we see a qualitative difference between the fourth and fifth order solutions: At fourth order (and also at third order) there appears a periodic orbit of winding number $\frac{3}{4}$, hence we see 3 elliptic points at the $I_1 = 0$ section and 4 elliptic points at the $I_2 = 0$ section. Among the elliptic points seen in the sections there are hyperbolic points denoted by h. In the vicinity of the hyperbolic points there are chaotic orbits. This chaos is fictitious and vanishes when we use fifth or higher order models.

We have developed a computer program which finds the periodic points of the map with prescribed period and computes their Floquet exponents. Computations were made for the case of pure gravity

Table 1
Demonstration of convergence for the point s in fig. 1.

Order	$R1$	$R2$	Residue
2	4.004 517	0.872 757 8	0.8706
3	4.007 515	0.862 972 0	0.9827
4	4.018 689	0.825 410 3	0.9832
5	4.017 307	0.830 156 2	0.9809
6	4.016 362	0.833 382 5	0.9801
7	4.016 644	0.832 418 5	0.9800
8	4.016 758	0.832 030 1	0.9803
9	4.016 698	0.832 237 2	0.9804

waves with $k_2/k_1 = 2$, and an Hamiltonian that is equal to 97% of H_c. Note that for the two-modes "Stokes wave" associated with $H = 0.97H_c$, the steepness height/λ is 0.152 compared to 0.208 for the maximal Stokes wave, max($\eta(x)$/height) is 0.622. The computations for the $I_2 = 0$ section show that for all orders of solutions there is one family of periodic points of perid 2 denoted by s (Stokes), and that these points are elliptic; there are no hyperbolic points of period 2. The computations show also that for all orders there are no periodic points with periods 3, 5 or 6. Periodic points of period 4 (elliptic as well as hyperbolic) exist in solutions of order three and four (these are seen in fig. 1); in the higher order solutions they disappear. The minimum period of the hyperbolic points, which exists in solutions of all orders, is 7. There are four families of periodic points with period 7: two families of elliptic points and two families of hyperbolic points. The winding number of this orbit is $\frac{5}{7}$ and it can be seen as a period 5 orbit in the $I_1 = 0$ section in fig 1a. It must be mentioned that the chaotic regions, associated with hyperbolic points of period 7, are extremely small and very difficult to resolve.

4.3. *Resonance and true chaos*

We expect a strong interaction to occur under resonance conditions. The lowest order resonance that can be attained for deep water gravity waves with dispersion relation $\omega = \sqrt{gk}$ is for $k_2 = 4k_1$. The frequency ratio is then $\omega_2 = 2\omega_1$. From the waves with wavenumbers $\pm k_1, \pm k_2$ we may form (with repetitions) a resonant quintet:

$$(-k_1) - 3k_1 + k_2 = 0; \quad \omega_1 - 3\omega_1 + \omega_2 = 0 .$$

Hence, we expect strong interaction via fourth order terms (which are present, however, in lower order models as well, through secondary interactions). It turns out, that for this case we have two primary stable periodic trajectories, e_1, e_2, which correspond on the Poincaré map $I_1 = 0$ to elliptic periodic points of period one. The islands of closed curves, surrounding such elliptic points, are shown in fig. 2a. The separatrix, which separates the islands surrounding different solutions is shown in fig. 2b. This separatrix is homoclinic to hyperbolic periodic points, h_1, which leads to the onset of local chaos, shown in the magnified picture in fig. 2b′.

For the chaotic region the divergence of a pair of nearby trajectories was computed. The results, presented in fig. 2c and d, show the exponential divergence of trajectories. Dark areas arise due to fast oscillations. The computation was carried out to seventh order which we consider very accurate. Fig. 2e shows the form of the free surface for the two types of standing waves, denoted in fig. 2a by s and h_1. The new kind of wave, h_1, is currently investigated using higher order models with more modes. The steepness of the waves in fig. 2e is much smaller than that of figs. 2a–2d, in order to lessen the instability associated with the h_1 type (the acceleration in the h_1 wave presented is almost $-\frac{2}{3}$ g).

4.4. *The two-dimensional case*

Truncation to a two-modes model in a form similar to that given in section 3.2 was carried out also for the two-dimensional case. The only change is that the coefficients in (3.18), (3.19), (3.20) were obtained by collecting terms in the appropriate two-dimensional equations. Introduction of spatial modes (3.6), (3.7) provides new possibilities for resonant interactions. We restrict ourselves to the case of deep-water pure gravity waves in a square basin. The mode frequency depends only on the modulus of k. Thus for each $k = (\pi n/L, \pi m/L)$, $m \neq n$ exists $k' = (\pi m/L, \pi n/L)$ and $\omega(k) = \omega(k')$. It is clear,

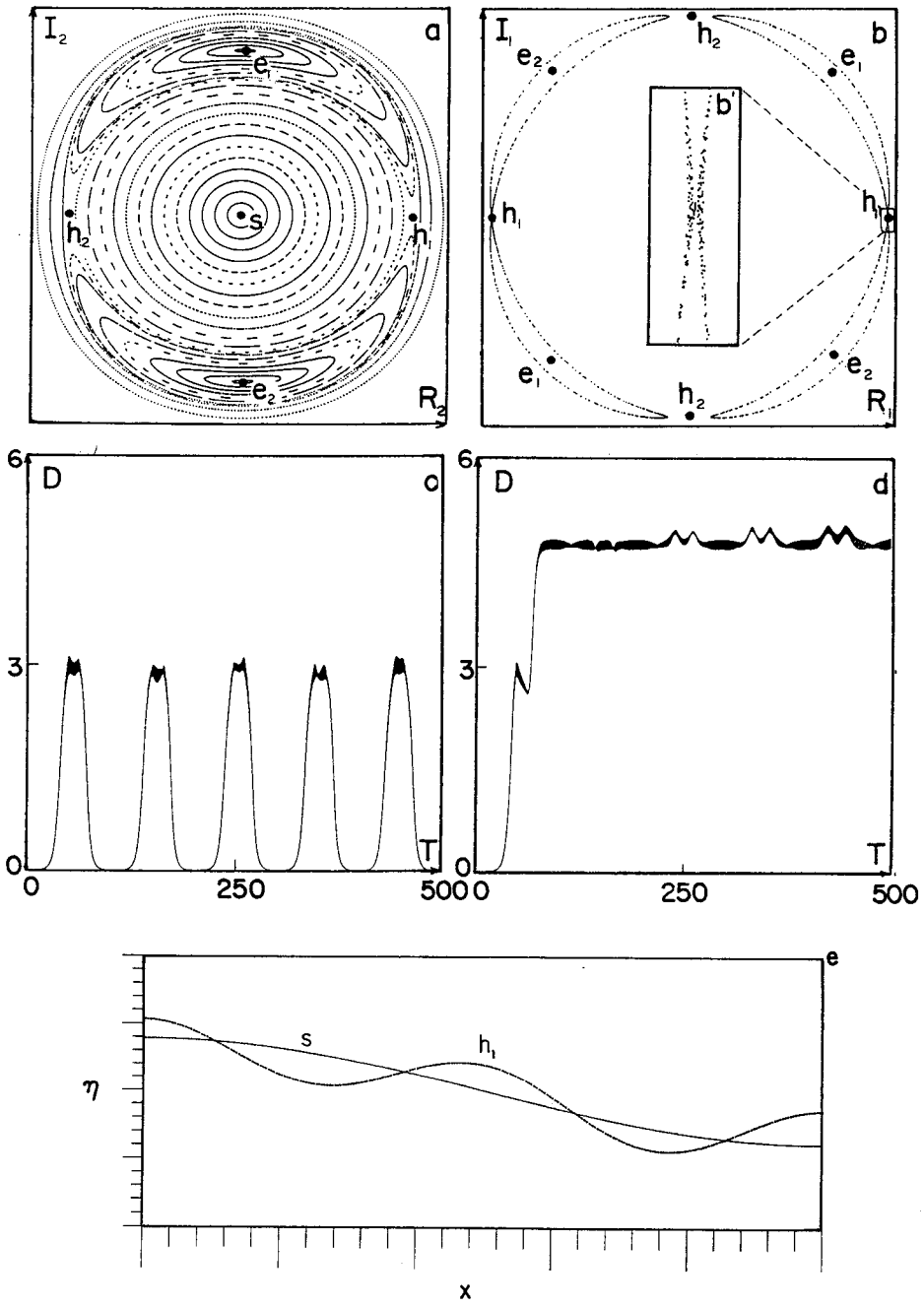

Fig. 2. Resonance for gravity waves with $k_2 = 4k_1$, $\omega_2 = 2\omega_1$. Seventh order solution. For classification of points see fig. 1. (a) $I_1 = 0$ Poincaré section. (b) Separatrix through h_1 on the $I_2 = 0$ section. Initial condition: $\varepsilon_1 = 0.058$, $\varepsilon_2 = 0.133 < \varepsilon_c$. (b') Magnified chaotic part of a near separatrix trajectory. (c), (d) The divergence D of a pair of nearby trajectories as function of time T (in wave periods), initiating at the vicinity of h_1, h_2 respectively. Initial distance $D(0) = 10^{-5}$. (e) The free surface displacements of the standing waves of types s and h (steepness of the h_1 wave is 0.098).

that due to full symmetry in this case the Poincaré sections $I_1 = 0$ and $I_2 = 0$ are identical. A typical example of this resonant picture is given in fig. 3.

For this specific case $\boldsymbol{k}_1 = (0, \pi/L)$, $\boldsymbol{k}_2 = (\pi/L, 0)$. The resonant structure is here very clear: we have three elliptic fixed points, (e_0, e_1 and e_2) and two hyperbolic fixed points (h_1, h_2).

A magnified part of the trajectory near the separatrix through h_2 is shown in fig. 3b. Note that in this

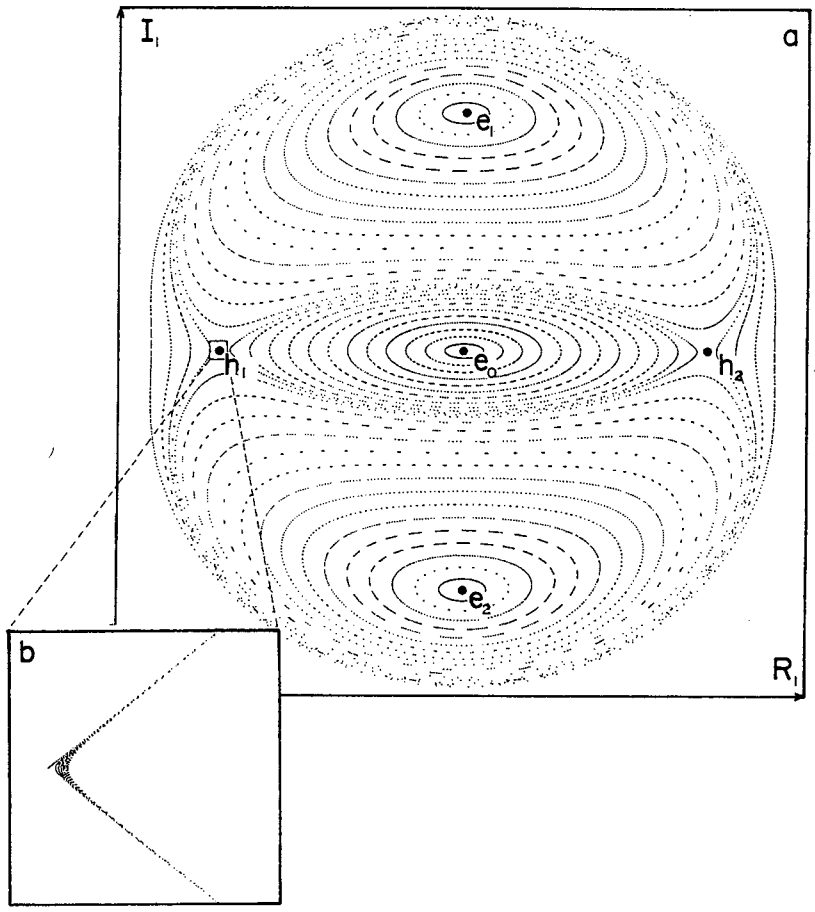

Fig. 3. Cross resonance in a square basin. $H = 0.2H_c$, $k_1 = (1, 0)$, $k_2 = (0, 1)$, $\omega_1 = \omega_2$. Seventh order solution. (a) Poincaré section $I_2 = 0$. (b) Magnified chaotic part of trajectory initiating near the point h_1.

case we have significant energy exchange between the two modes, due to significant excentricity of the central family of ellipses. This picture was obtained for the case, where the angle μ between k_1 and k_2 is equal to $\frac{1}{2}\pi$.

As can be seen from the symmetry conditions (3.4), this is the maximum possible value for the angle between k_1 and k_2.

When the angle μ decreases, the picture changes: the central family of ellipses becomes more and more flat, approaching a straight line, and for some critical value of μ, which is sensitive to the order of solution, a bifurcation occurs. The central elliptic point, e_0 becomes hyperbolic, and the hyperbolic points h_1 and h_2 become elliptic.

Therefore, for some values of μ the solutions of different orders give qualitatively different pictures (see fig. 4). We can see again that the third-order approximation is not good enough, and at least a fifth-order solution must be used. Fig. 4 is for $H = 0.8H_c$. The results for much smaller H are qualitatively the same. However, for this case the central part of the figure (around $I_1 = 0$) is extremely narrow and difficult to resolve.

A similar interesting case is that of near resonance, where $k_1 \approx k_2$. It can be shown that such near-resonant picture with hyperbolic fixed points of period 1 exists for $\omega_1/\omega_2 \in (1 - \alpha, 1 + \alpha)$, where α depends on the magnitude of the Hamiltonian H. An individual mode k_2 is stable to disturbances with

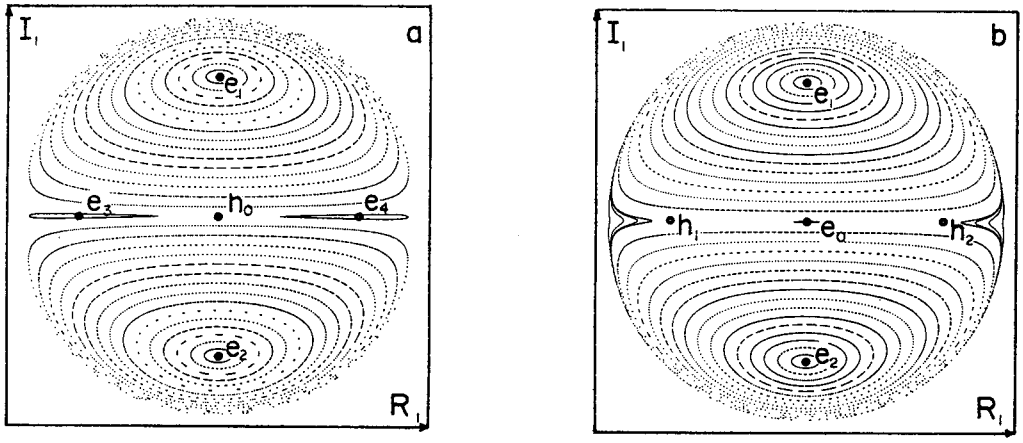

Fig. 4. Poincaré $I_2 = 0$ sections for cross resonance in a square basin. $H = 0.8H_c$, $k_1 = (17, 28)$, $k_2 = (28, 17)$, $\omega_1 = \omega_2$. (a), (b) Third and fifth order solution, respectively. Note the change in the nature of the stationary points.

wave vector k_1 when the central point of the section $I_2 = 0$, e_0 in fig. 3a, is elliptic. One can show that there exists $\beta = \beta(H, \omega_1/\omega_2)$ such that for $\omega_1/\omega_2 \in (1 - \alpha, 1 + \alpha)$ and $\mu \in (0, \beta)$ this central point is hyperbolic. It should be noted that the near-resonant conditions may exist also for the one-dimensional case, when sufficiently large k_1 and $k_2 = k_1 + \pi/L$ are taken. For the two-dimensional case the near-resonant condition exists for considerably smaller values of $|\boldsymbol{k}|$.

The above-mentioned phenomenon can serve as a possible mechanism for the angular spread of energy.

5. Conclusions

The main conclusion of this work is that high order approximations of the water-wave problem are "a must" for reliable studies of transition from order to chaos. We have derived the necessary model equations and present them in full details.

From the examples presented in section 4 we draw the following observations.

(i) Low order expansion can generate fictitious chaos which disappears when higher order terms are included. In fig. 1 we demonstrate this fact for local chaos. To obtain this phenomenon for global (in contrast with local) chaos we need to increase the wave steepness beyond the physically admissible limit. Such results are shown in fig. 5.

(ii) True local, but significant, chaos is possible for resonance and near-resonance conditions. This occurs for rather energetic but still physical systems, as we have clearly demonstrated in sections 4.3 and 4.4.

(iii) It is rather difficult to give a recipe for the recommended order one should use. From the examples presented herein, as well as from additional examples, including cases of gravity capillary waves, that we have studied in [12]; we give in table 2 estimates of the "optimal" order of the model for different ranges of ε_{max}.

Finally, the main drawback of our calculations is the restriction to two-modes. At present we are working to resolve the numerical and graphical difficulties, related to the multi-mode problem. Note that for three or more modes, new effects are expected, the most important is Arnold diffusion [1]. For this case, resonant layers are no longer isolated by KAM surfaces and they intersect, forming a

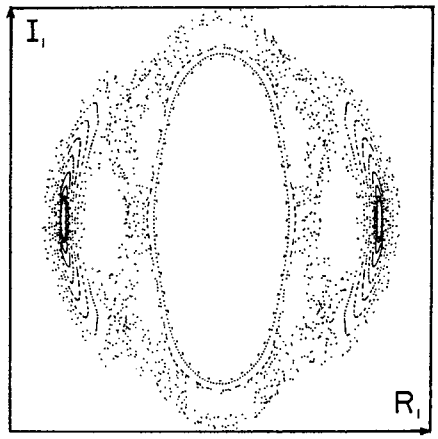

Fig. 5. Global chaos: $I_2 = 0$ section at second order. $k_2 = 2k_1$. This example is of theoretical value only, since $H = 3H_c$.

Table 2
Guidelines for order of model to be used.

Range of $\varepsilon_{max}/\varepsilon_c$	Recommended order of the model	
	gravity capillary waves	gravity waves
0.0–0.5	3	3
0.5–0.7	5	3
0.7–0.8	7	5
0.8–0.9	9	5

connected web. The interconnection of the dense set of layers ensures, that the stochastic motion, stepping from layer to layer, can carry the system arbitrarily close to any region in the phase space consistent with energy conservation.

Acknowledgement

This study is supported by the US Office of Naval Research, Grant No. N00014-91-J-1449.

Appendix A. Expressions for the interaction coefficients

Coefficients for eq. (2.14):

$$A_0 = -1\,, \quad A_q = -\sum_{n=1}^{q} \frac{\sigma_{q-n}^n}{n! w^n} \frac{\mu(\sigma_{q-n}, n)}{\mu(\sigma_{q-n}, 0)} A_{(q-n)}\,, \tag{A.1}$$

where

$$\sigma_{q-n} = \left| \sum_{j=0}^{q-n} \boldsymbol{k}_j \right|\,, \quad \mu(\sigma_{q-n}, n) = \tfrac{1}{2}[\exp(\sigma_{q-n}h) + (-1)^n \exp(-\sigma_{q-n}h)]\,. \tag{A.2}$$

The values of w for the following different cases are: $w = 2\pi$ for the continuous two-dimsional case,

$w = \sqrt{2\pi}$ for the continuous one-dimensional case, $w = \sqrt{L_1 L_2}$ for the discrete two-dimensional case, $w = \sqrt{L_1}$ for the discrete one-dimensional case, where L_1 and L_2 are dimensions of a rectangular basin.

Coefficients for eq. (2.15):

$$B_q = -\sum_{n=0}^{q} \frac{\sigma_{q-n}^{n+1}}{n! w^n} \frac{\mu(\sigma_{q-n}, n+1)}{\mu(\sigma_{q-n}, 0)} A_{(q-n)} . \tag{A.3}$$

Coefficients for eq. (2.17):

$$C_0 = B_0 , \quad C_1 = B_1 + \frac{\boldsymbol{k}_0 \cdot \boldsymbol{k}_1}{w} , \quad C_q = B_q - B_{(q-2)} \frac{\boldsymbol{k}_{q-1} \cdot \boldsymbol{k}_q}{w^2} \quad (q \geq 2) . \tag{A.4}$$

Coefficients for eq. (2.20) and (2.23):

$$G_q = \frac{\gamma_g'}{w^{2q}} (\boldsymbol{k}_0 \cdot \boldsymbol{k}) \left(\prod_{m=1}^{q} (\boldsymbol{k}_{2m-1} \cdot \boldsymbol{k}_{2m}) \right) , \tag{A.5}$$

where

$$\gamma_n' = \frac{1}{2^n n!} \prod_{m=1}^{n} (2m-1) , \quad \beta_{n+1}' = \gamma_n' \frac{1}{2(n+1)} . \tag{A.6}$$

Coefficients for eq. (2.26):

$$D_0 = \frac{1}{w} \left[B_0 \binom{0}{0} B_0 \binom{1}{1} + \boldsymbol{k}_0 \cdot \boldsymbol{k}_1 \right] , \quad D_1 = \frac{1}{w} \left[B_0 \binom{0}{0} B_1 \binom{2}{1} + B_1 \binom{1}{0} B_0 \binom{2}{2} \right] ,$$

$$D_q = \frac{1}{w} \left[\sum_{j=0}^{q} B_j \binom{j}{0} B_{(q-j)} \binom{q+1}{j+1} - \frac{1}{w^2} \sum_{j=0}^{q-2} B_j \binom{j}{0} B_{(q-2-j)} \binom{q+1}{j+3} \boldsymbol{k}_{j+1} \cdot \boldsymbol{k}_{j+2} \right] \quad (q \geq 2) , \tag{A.7}$$

where $B_q \binom{q+\alpha}{\alpha}$ is calculated using (A.3) after replacing σ_{q-n} by the new expressions

$$\sigma_{q-n} = \left| \sum_{j=0}^{q-n} \boldsymbol{k}_j \right| \quad \text{for } \alpha = 0 , \qquad \sigma_{q-n} = \left| \sum_{j=\alpha+n}^{q+\alpha} \boldsymbol{k}_j \right| \quad \text{for } \alpha > 0 . \tag{A.8}$$

Appendix B. A necessary condition for convergence

Here we present an analytic derivation of a necessary criterion for the convergence of the series on the rhs of the evolution equation (3.12). The simplest case arises when the system is truncated to a single mode. The resulting series is a subseries of any series for a greater number of modes. The convergence of the subseries, which describes the self-interaction of a single mode is a necessary condition for the convergence of the whole series; and if these subseries diverge, the whole series will in general divergence too.

For the single mode case we have

$$\eta(x, t) = A \cos(k_l x) \rho(t) , \quad \rho(t) = \mathcal{O}(1) , \tag{B.1}$$

$$\psi(x, t) = \frac{A}{\lambda^2} \cos(k_l x)\, \theta(t)\,, \quad \theta(t) = \mathcal{O}(1)\,, \tag{B.2}$$

where λ is given in (2.22b) and

$$A_l = \max_{t_0<t<\infty} (|\hat{\eta}(k_l, t)|)\, \frac{2}{\sqrt{L_1}}\,. \tag{B.3}$$

We define

$$\varepsilon_l = \frac{A|k_l|}{2\pi}\,, \tag{B.4}$$

and hence

$$\max_{t_0<t<\infty} (|\rho(t)|) = \max_{t_0<t<\infty} (|\theta(t)|) = 1\,. \tag{B.5}$$

After taking the Fourier transforms of (B.1) and (B.2) and switching to R and I, using (2.21), we have

$$R_l = \frac{\varepsilon\pi\sqrt{L_1}}{\sqrt{2}\,\lambda_l|k_l|}\,\rho(t)\,, \quad I_l = \frac{\varepsilon\pi\sqrt{L_1}}{\sqrt{2}\,\lambda_l|k_l|}\,\theta(t)\,. \tag{B.6}$$

We denote

$$C'_q = C_q L_1^{q/2}\,, \quad D'_{q-1} = D_{q-1} L_1^{q/2}\,, \quad G'_{q/2} = G_{q/2} L_1^{q/2}\,. \tag{B.7}$$

The equation of self-interaction obtained from (3.12) is written as follows:

$$\begin{aligned}
\rho_t + \mathrm{i}\theta_t + \mathrm{i}\omega(\rho + \mathrm{i}\theta) = {} & \frac{|k_l|}{\lambda^2} \sum_{q=1}^{\infty} \sum_{l_0 \ldots q \in \{-l, l\}}^{q+1} C'_q \frac{(\varepsilon\pi)^q}{|k_l|^{q+1}}\, \theta\rho^q\, \delta\Big[k_l, \sum_{j=0}^{q} k_{l_j}\Big] \\
& + \frac{\mathrm{i}|k_l|}{\lambda^2} \sum_{q=1}^{\infty} \sum_{l_0 \ldots q \in \{-l, l\}}^{q+1} D'_{q-1} \frac{(\varepsilon\pi)^q}{|k_l|^{q+1}}\, \theta^2\rho^{q-1}\delta\Big[k_l, \sum_{j=0}^{q} k_{lj}\Big] \\
& - \mathrm{i}s\lambda^2|k_l| \sum_{q=1}^{\infty} \sum_{l_0 \ldots q \in \{-l, l\}}^{q+1} G'_{q/2} \frac{(\varepsilon\pi)^q}{|k_l|^{q+1}}\, \rho^{q+1}\delta\Big[k_l, \sum_{j=0}^{q} k_{l_j}\Big]\,,
\end{aligned} \tag{B.8}$$

where $\lambda = \lambda(k_l)$.

The last term in this equation can be evaluated exactly using Stirlings formula. The condition for convergence of this term is

$$\varepsilon \le \frac{1}{2\pi}\,. \tag{B.9}$$

For the other two terms the behavior of the coefficients $C''_q = C'_q/|k_l|^{q+1}$ and $D''_{q-1} = D'_{q-1}/|k_l|^{q+1}$ was studied numerically up to order 23. These calculations show, that the average values of C'' and D'' decay, but not exponentially. Thus the limitation on ε in all the terms in (B.8) is the same

$$\varepsilon \leq \frac{1}{2\pi} .$$

The detailed consideration can be found in [12].

References

[1] V.I. Arnold, Small divisor problems in classical and celestial mechanics, Russian Math. Surveys, 18 (1965) 85–192.
[2] T.B. Benjamin, Impulse, flow-force and variational principles, IMA J. Appl. Math. 32 (1984) 3–68.
[3] W. Craig, Water waves, Hamiltonian system and Cauchy integrals. Microlocal Analysis and Nonlinear Waves (eds. M. Beals, R. Melrose and J. Rauch), IMA Volumes in Mathematics and its Applications, Vol. 30 (Springer, 1989) pp. 37–45.
[4] D.G. Dommermouth and D.K.P. Yue, A high order spectral method for the study of nonlinear gravity waves, J. Fluid Mech. 184 (1987) 267–288.
[5] H. Goldstein, Classical Mechanics, 2nd Ed. (Addison-Wesley, Reading, MA, 1980).
[6] K. Hasselman, On the nonlinear energy transfer in gravity-wave spectrum. 1. General theory, J. Fluid Mech. 12 (1962) 481–500.
[7] R.S. MacKay, Introduction to the dynamics of area-preserving maps, in: Proc. US Particle Accelerator School, SLAC, ed. M. Month (1985).
[8] J.W. Miles, On Hamilton's principle for surface waves, J. Fluid Mech. 83 (1977) 153–158.
[9] F.C. Moon, (1987). Chaotic vibrations, an introduction for applied scientists and engineers (John Wiley, 1987) 305 p.
[10] W.J. Pierson, Wind generated gravity waves, Adv. Geophys. 2 (1955) 93–178.
[11] M. Stiassnie and L. Shemer, On modifications of the Zakharov equation for surface gravity waves, J. Fluid Mech. 143 (1984) 47–67.
[12] M. Stiassnie, Y. Agnon and M. Glozman, Order and chaos in standing surface waves, First annual scientific report, Coastal and Marine Engineering Research Institute, Technion, Haifa, Israel, P.N. 290/91 (1991).
[13] B.J. West, K.A. Brueckner, and R.S. Janda, A new numerical method for surface hydrodynamics, J. Geophys. Res. C 92 (1987) 11 803–11 824.
[14] H.C. Yuen and B.M. Lake, Nonlinear dynamics of deep-water gravity waves, Adv. Appl. Mech. 22 (1982) 67–229.
[15] V.E. Zakharov, Stability of periodic waves of finite amplitude on the surface of deep fluid, J. Appl. Mech. Tech. Phys. 2 (1968) 190–194.
[16] J.A. Zufiria, Oscillatory spatially periodic weakly nonlinear gravity waves on deep water, J. Fluid Mech. 191 (1988) 341–372.